120 Gbit/s Over 500-km Using Single-Band Polarization-Multiplexed Self-Coherent Optical OFDM

Brendon J. C. Schmidt, Zuraidah Zan, Liang B. Du, and Arthur J. Lowery, *Fellow, IEEE*

Abstract—In this paper, we experimentally demonstrate a single-band self-coherent polarization-multiplexed optical orthogonal frequency-division multiplex system with a raw data rate of 120 Gbit/s. The transmitter uses a novel RF structure that eliminates the need for RF mixers and optical filters. The receiver uses a novel architecture where the optical carrier is filtered and amplified for self-coherent detection. The receiver is polarization diverse and allows for the usual frequency guard band between the carrier and the sideband to be reduced in width, thus increasing spectral efficiency. Using two commercial 20 GS/s arbitrary-waveform generators to generate a single information-carrying band per polarization, we achieve a raw data rate of 120 Gbit/s over 500 km of standard single-mode fiber.

Index Terms—Chromatic dispersion, compensation, direct detection, orthogonal frequency-division multiplexing (OFDM), optical single sideband (OSSB), polarization multiplexing, self-coherent.

I. INTRODUCTION

THE rapidly increasing traffic demands in long-haul optical fiber communications have caused considerable interest in alternative modulation formats that can efficiently use the capacity of standard single-mode fiber (SSMF) [1]. As 100 Gbit Ethernet (100 GbE) is set to become the next standard for IP transport, next-generation optical systems need to be able to transport 100 GbE in a single wavelength [2]. Differential quadrature phase-shift keying (DQPSK) using polarization-division multiplexing (PDM) and either direct or coherent detection [3] are possible solutions. Recent demonstrations of PDM-8PSK [4] using coherent reception and offline DSP achieved a high tolerance for chromatic dispersion (CD) and polarization-mode dispersion (PMD).

Another modulation format that has attracted considerable interest for long-haul transmission is optical orthogonal frequency-division multiplexing (O-OFDM) [5]–[7]. This format has many advantages: 1) it can adaptively compensate for very

high levels of CD [5] and PMD [8]; 2) the computational complexity scales well with increasing data rate [1]; and 3) the signal has a well-defined optical spectrum with high spectral efficiency [9], [10]. Recently, there have been several demonstrations that show the potential of O-OFDM for next-generation 100-Gbit/s systems. O-OFDM using coherent reception (CO-OFDM) and PDM has been used to achieve 100 GbE data rates over 1000 km [11], [12]. In both demonstrations, the wideband optical signal was generated by multiplexing a number of narrower signal bands (subbands) together. In [11], the bands were generated in the optical domain by modulating a comb of laser lines, similar to ''coherent wavelength division multiplexing (WDM)''[13] but with OFDM modulation of each line. In [12], the bands were generated in the electrical domain and then upconverted to selected intermediate RFs before optical modulation. The use of multiple bands allows the sampling rate of the digital-to-analog converters (DACs) to be reduced, and reduces some OFDM overheads [12]. However, these benefits come at the cost of transmitter complexity. Both systems require multiple DACs; optical multiplexing requires multiple optical modulators and RF multiplexing requires multiple electrical mixers. There are also ''all-optical'' versions of O-OFDM [14], using no digital processing at the transmitter. These similarly require multiple optical modulators.

In this paper, we demonstrate a 120-Gbit/s self-coherent O-OFDM (SCO-OFDM) system that uses only one signal band per polarization; a 100-Gbit/s version of this system was presented at the Optical Fiber Communication Conference and Exposition (OFC) 2009 [15]. The system does not use subbands in either the RF or optical domains. The use of direct detection [16] means that a laser "local oscillator" is not required at the receiver. Single-band schemes have far simpler RF and optical paths in the transmitter but are limited by the performance of the transmitter DACs. We have aimed at achieving the maximum performance from second-generation arbitrary waveform generators (AWGs) as of May 2009.

Our system uses a polarization-diverse receiver [17], unlike alternative direct-detection receivers presented at the OFC/National Fiber Optic Engineers Conference (NFOEC) 2009 postdeadline sessions [18]. This means that the performance of PDM is not degraded in high-PMD optical links. The system has also a number of novel features developed by our group, including a transmitter with no RF mixers or optical filters [19], carrier boost to improve receiver sensitivity [20], and the polarization-diverse receiver itself [17]. The system uses a reduced ''gap'' [21] between the transmitted carrier and the OFDM sideband,
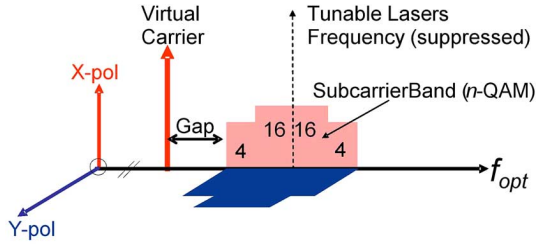
Fig. 1. Desired output spectrum of the transmitter.

Fig. 2. Optical OFDM transmitter for a single polarization.

which is possible through the use of balanced detectors at the receiver. This reduced gap improves the spectral efficiency dramatically, compared with a direct-detection O-OFDM system (DDO-OFDM) [16], but retains its tolerance to phase noise from the transmitter's laser. In contrast, CO-OFDM is sensitive to laser phase noise unless phase compensation techniques [22] or narrow-linewidth lasers and pilot tones [23] in the OFDM symbol are used.

The paper is organized as follows. Section II describes the key features of the system. Section III provides the experimental details. In Section IV, we present and discuss the results and compare them to the results from simulation. In Section V, we present our conclusions.

II. SYSTEM DESIGN THEORY

This section covers the design concepts used in the system to achieve a wide modulation bandwidth with low sample rates at the transmitter and polarization diversity at the receiver.

A. Transmitter Design

SCO-OFDM, like DDO-OFDM, requires an optical carrier to be transmitted along with the OFDM subcarriers. This carrier mixes with the optical subcarriers at the photodiode to produce a set of electrical subcarriers. Since the carrier and the subcarriers are derived from the same laser source, the phase noise of the source (due to laser linewidth) will cancel upon detection, provided there is little differential delay between the carrier and the subcarriers.

Fig. 1 shows the desired optical spectrum for a polarization-multiplexed DDO-OFDM transmitter. This comprises subcarrier bands in orthogonal polarizations, together with an optical carrier in one (or other) of the polarizations. In this figure, the OFDM subcarriers are modulated with 16-quadratic-amplitude modulation (QAM) in the center of the subcarrier band and 4-QAM at the edges of the subcarrier band, though other arrangements are possible. The source could be a tunable laser (to allow the transmitter to be adjusted to any wavelength). A virtual carrier is created by frequency-shifting the tunable laser line to one side of the subcarrier band [19]. A "gap" is left in the spectrum. In most DDO-OFDM systems [21], the gap ensures that intermixing products between subcarriers, caused by photodetection, fall below the subcarriers' frequency band: in the receiver design presented later, the gap's purpose is to allow the carrier and subcarrier bands to be separated using optical filters.

The spectrum of Fig. 1 can be generated by applying the inphase (I) and quadrature (Q) components of the electrical OFDM signal to a complex optical modulator (also known as a QPSK modulator, optical single-sideband modulator, or cascaded triple Mach–Zehnder interferometric (MZI) modulator). This arrangement is shown in Fig. 2. The electrical OFDM signal is generated by presenting parallel data to a set of QAM modulators. The QAM modulators' outputs then become the (frequency domain) inputs to an inverse fast Fourier transform (IFFT). The output of the IFFT is a superposition of subcarriers, each corresponding to a frequency input of the IFFT. These are converted to a complex serial data stream and a cyclic prefix (CP) is added.
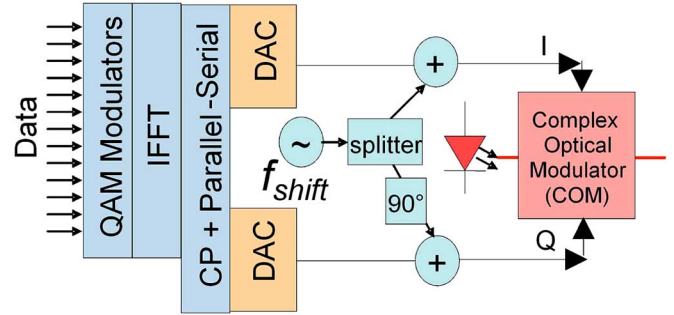
The optical modulator is biased at null power so that the optical field is proportional to the electrical drive voltage [24]. This ensures a one-to-one mapping of the optical and electrical spectra, both at the transmitter and the receiver. This is necessary to enable fiber dispersion to be equalized electrically on a subcarrier-by-subcarrier basis. The virtual carrier is generated by frequency-shifting the original line. This can be achieved by adding sine and cosine waveforms to the two inputs of the complex optical modulator, so that it operates as a single-sideband modulator to create a single sideband comprising the virtual carrier. The frequency shift is equal to the frequency of the oscillator, f_{shift}. The power in the optical carrier can be controlled simply by the amplitude of the RF waveform and the frequency gap by adjusting its frequency. This is very convenient experimentally and allows a flexible transmitter module to be manufactured.

An advantage of the transmitter design in Fig. 2, over previous designs, is that it provides the maximum possible optical subcarrier-band bandwidth for a given sample rate [19]. Neglecting the narrow guard bands required for antialiasing filtering, the bandwidth of the optical subcarrier band can equal the sample rate of the DACs. For example, 20 GS/s DACs will give a total subcarrier bandwidth approaching 20 GHz, which could support close to 40-Gbit/s (per polarization) using 4-QAM modulation, or 80 Gbit/s per polarization with 16 QAM. These data rates do not include forward error correction (FEC) overheads or the CP overhead. Alternative approaches generate the virtual carrier by setting the inputs of the IFFT appropriately [25], so one half of the double-sided spectrum is sacrificed for the gap and the carrier, or by frequency-shifting the electrical subcarrier band away from the laser line using RF mixers [21]. Schemes using RF mixers are undesirable because they are expensive and can introduce nonlinear distortion to the signal, and have limited bandwidths. Also, it is desirable to place the subcarrier band around dc of the modulator's electrical response (at positive and
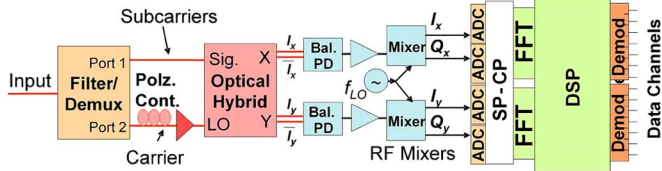
Fig. 3. Dual-polarization optical OFDM receiver.

negative frequencies around dc), because this is where it has its maximum efficiency and flatness. RF mixers would use the modulator at some intermediate frequency, and the IFFT generated spectrum uses only positive frequencies for the subcarriers. The virtual carrier is placed at a very high frequency (f_{shift}) in our scheme. The low efficiency of the optical modulator at this frequency is not important, because powerful *narrowband* high-frequency RF amplifiers are readily available to compensate for this low efficiency.

Two signal polarizations can be generated by combining the outputs of two transmitters, each with a polarization beam combiner, as shown in Fig. 2. A desirable simplification is to remove the carrier generation feature from one transmitter; otherwise, the two carriers will have a random phase shift, and thus create a carrier with a random polarization state. One carrier is easily removed by removing one transmitter's sinusoidal generator. Another desirable simplification is to use a single tunable laser for both polarizations, as this will ensure that the bands of both polarizations have phase fluctuations correlated with the common carrier, so these phase fluctuations will cancel upon photodetection.

B. Receiver Design

We use an improved version of the high-performance receiver of [17], using balanced photodetectors rather than single-ended photodetectors. This receiver reduces the sensitivity limitations of conventional direct-detection receivers [26], allows polarization multiplexing and PMD compensation, and maintains direct-detection receiver's insensitivity to laser linewidth by using self-carrier extraction [27], [28]. The balanced photodetection rejects unwanted spectral components, including the intermixing of subcarriers with other subcarriers. This allows a reduced frequency gap, and thus gives an increased spectral efficiency.

The topology of the receiver is shown in Fig. 3. The first stage (filter/demux) comprises two optical filters to separate the carrier and sideband spectral components. The filter also provides amplified spontaneous emission (ASE) bandwidth limiting to reduce shot noise. The separated carrier and sideband signals are then optically pre-amplified and drive the inputs of the polarization-diverse optical hybrid. The hybrid has an internal polarization beam splitter on the signal input and an internal linear polarizer on the LO input. The linear polarizer ensures equal carrier power for each polarization and the polarization controller maximizes carrier output.

The hybrid provides balanced inphase outputs for the X and Y polarizations: the receiver is a heterodyne rather than a homodyne design, so the I and Q components are recovered using RF mixers. The X and Y polarization outputs of the optical hybrid are detected with balanced photodetectors, in contrast to [17]. These strongly suppress *subcarrier* $\times$ *subcarrier* mixing
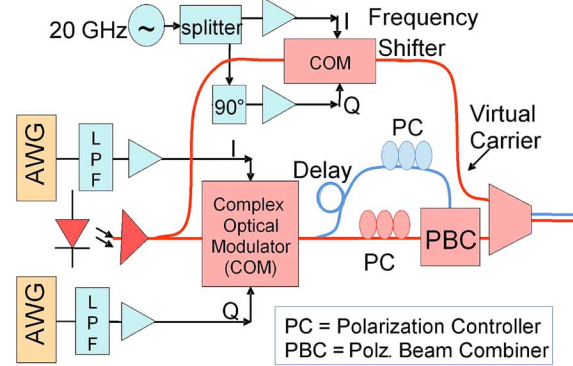
Fig. 4. Transmitter as implemented using commercial components.

products [26], which would normally fall in the frequency gap in a direct-detection design. Thus, the width of the gap can be reduced to below the bandwidth of the subcarrier band without penalty, provided the optical filters are sharp enough. The balanced photodetectors also reject ASE $\times$ ASE components. The optical preamplification serves two functions: it increases the signal powers to minimize shot noise upon detection; boosting the carrier power [20] would allow unbalanced detection to be used [29], but in this design, it helps to reduce the impact of residual *subcarrier* $\times$ *subcarrier* mixing products caused by imbalances in the balanced detection. The detected outputs are then amplified and downconverted to the electrical baseband with two wideband electrical mixers. The I and Q outputs from each mixer are then low-pass filtered and captured by the four inputs of a digitizer. The digitized waveforms are converted to complex parallel data blocks and the CP is removed. The IQ compensation, channel estimation, and polarization demultiplexing are all performed in the DSP block, before the QAM symbols are demodulated into binary data.

III. EXPERIMENTAL DETAILS

The transmitter and the receiver described in Figs. 2 and 3 were constructed using commercial off-the-shelf components. This required some changes to their designs. Also, to save building two transmitters (one for each polarization), the X and Y polarization signals were generated using one modulator, then combined with a relative delay to decorrelate them. This section describes the implementation of the transmitter, receiver, and fiber link.

A. Implemented Transmitter

Fig. 4 shows the transmitter as implemented experimentally. The QAM coders, IFFT, and CP addition are all generated offline using MATLAB. The inphase component of the generated waveform is loaded into one Tektronix AWG7102 and the quadrature waveform into the other. The AWGs are used in interleaved and ''return-to-zero'' modes to provide an output sample rate of 20 GS/s each, with an analog signal bandwidth of approximately 6 GHz (-3 dB) and 10 GHz (-10 dB). Low-pass filters (LPFs) with sharp 10-GHz cutoffs are used to reduce the image band caused by the sampling process.

The outputs of the LPFs are amplified with 20-GHz bandwidth microwave amplifiers and fed to a Sumitomo

T-SBXI.5-20P 40-Gbit/s DQPSK optical modulator (a "complex optical modulator," COM). The source laser is a Photonetics Tunics external-cavity laser tuned to 1550 nm. An optical amplifier is used before the modulator to compensate for the low output power of this particular laser. The output of the modulator is split into two paths: one with a delay of either 54 or 64 ns, depending on the length of the CP. Polarization controllers (PCs) adjust the polarizations of the paths at the input to a polarization beam combiner (PBC). This combination emulates two separate transmitter cards, each supplying signals with orthogonal polarizations to one another.

The carrier could be generated in a similar manner to that shown in Fig. 2; however, the arrangement to generate two signal polarizations would cause the carrier and a delayed and rotated version of itself to be transmitted. We found that this causes the carrier at the receiver to change polarization rapidly (because the "blue" delay path and the "red" straight path will fluctuate in relative phase length due to vibrations), and the polarization at the receiver cannot be manually controlled. Thus, the carrier is actually generated by a separate modulator acting as a frequency shifter and added to the output of the PBC. This removed all the problems of a rapidly changing carrier polarization.

It is important to generate the I and Q waveforms with a precise phase relationship; otherwise, there will be leakage from the upper sideband to the lower sideband of the subcarriers, causing a large penalty. To achieve this, the AWGs are synchronized using a common clock and trigger source. This achieves a long-term mean offset of 1 ps and an rms timing jitter of 4 ps, as measured on a Tektronix 72004 DSO. The AWGs' roll offs, and large frequency response ripples in "interleaved" and "zeroed" modes are compensated by multiplying the inverse of each AWG's channel response with the QAM transmission data in the frequency domain, before the IFFT. This leads to a flat response, but the preemphasis causes a loss of DAC resolution. This loss, combined with the SNR penalty caused by using the DAC in "zeroed mode" (which is "return to zero" after each sample) causes the electrical SNR at the transmitter to be a major impairment to the bit error rate (BER) performance of the system. The electrical SNR impairments can be reduced by using the well-known bit loading techniques [30]. For this reason, a combination of 16 QAM was used for the center subcarriers and 4 QAM for the higher frequency subcarriers.

B. Fiber Link

The fiber plant uses seven spans of Corning SMF-28e: 1×50 km, 5×80 km, and 1×50 km for a transmission distance of 500 km with no dispersion compensation. LightWaves2020 erbium-doped fibre amplifiers (EDFAs) are used between each span. The input power into each span was set to approximately 0 dBm.

C. Implemented Receiver

The output of the final span is optically amplified and fed to the common port of a programmable optical filter (Finisar "Waveshaper 4000E"). The carrier and sideband spectral components are separated by the optical filters and routed to separate output ports. A filter with a 12-GHz full-width at half-maximum

TABLE I
KEY PARAMETERS OF THE EXPERIMENTAL SYSTEM

Subcarrier Band	4-QAM	16-QAM	Unit
# Subcarriers	360	598	-
Subcarrier BW	7.0	11.7	GHz
Data Rate (dual pol.)	28.1	93.4	Gbit/s
Total Subcarrier BW		18.8	GHz
Total Signal BW		29.4	GHz
Total Data Rate		121.5	Gbit/s

(FWHM) is used to separate the carrier; a 20-GHz filter extracts the sideband. The separated carrier is amplified to 15 dBm and the sideband to only 3 dBm to provide the equivalent of carrier boosting [20]. The amplified carrier and sideband are fed to the inputs of a Kylia MINT 2×8 optical hybrid. This can produce I and Q outputs for both the X and Y polarizations. However, as the carrier frequency is offset from the sideband, the hybrid was used as a heterodyne receiver, so only the inphase outputs for the X and Y polarizations are required.

Polarization control is required between the output of the carrier filter and the LO input of the optical hybrid to maximize the output carrier level. A manual controller was used in these experiments; however, a practical implementation would require a closed-loop controller. The outputs of the hybrid are fed into two U²T 40-GHz balanced photodetectors, one for each polarization. The photodetectors produced an electrical output with an intermediate frequency of 20 GHz, over a band from approximately 10 to 30 GHz. The outputs are each amplified with 40-GHz RF amplifiers (Marki A-0040) and then downconverted to the complex baseband with wideband IQ mixers (Marki). In [15], two independent 20-GHz sinewave generators were used: one at the transmitter for virtual carrier generation and the other at the receiver for electrical downconversion of the photodiode outputs. However, a common 20-GHz generator with split outputs for the transmitter and receiver ends did not affect the results, and all of the experiments in this paper use a single 20-GHz generator. The downconverted I_x, Q_x, I_y, and Q_y signals are sampled in real time by the four channels of a Tektronix 72004 20-GHz 50-GS/s oscilloscope. The samples are then analyzed in MATLAB, which includes algorithms for IQ imbalance correction [12], polarization demultiplexing, channel equalization, and QAM decoding.

IV. EXPERIMENTAL RESULTS

A combination of 4-QAM and 16-QAM subcarrier modulation is used to demonstrate the performance of the system. A raw data rate of 120 Gbit/s can be transmitted over a distance of 500 km of SSMF. This data rate is enough to cover the overheads for 100 GbE transmission. Table I shows the subcarrier allocations, bandwidths, and data rates contributed by the two modulation levels.

The experimental system operates using frames of data, which the AWGs repeat over and over from their memories. The frames are designed so that the signals can be equalized using the training within a single frame, which is a limitation imposed by offline processing. A frame comprises a training sequence of 60 OFDM symbols and a data payload of 150 symbols (467 000 random bits). The long training sequence

reduces the average data rate to 85 Gbit/s. This overhead can be reduced by using longer data payloads and using running averages over multiple frames to reduce the required length of each training symbol [12]. The techniques proposed in [31] would reduce the training overheads further.

The training is required to find the matrix coefficients for both IQ compensation and polarization demultiplexing at the receiver. As described in [12], the training for a single transmitter system with a delay line for decorrelation requires a few modifications. To enable polarization demultiplexing at the receiver, the training sequence begins with 30 OFDM training symbols interleaved with 30 empty symbols, then develops as follows: 1) the training components that travel directly to the X input of the polarization beam combiner become the training symbols for the X polarization and 2) the training components that travel via the delay line to the Y input of the polarization beam combiner become the training symbols for the Y polarization. The delay line causes the Y training symbols to occupy the previously empty symbol slots, and the training sequence after the polarization combiner becomes a set of 60 interleaved X and Y training symbols. The known training data and the received X and Y data can then be used at the receiver to demultiplex the X and Y data.

The data content of the 30 training symbols is selected to give low peak-to-average power ratios (PAPRs). The symbols are scaled to just below the clipping level for the payload data. This scaling increases the training symbol energy by 2.3 dB and helps offset the 3-dB power loss in the training sequence caused by the empty symbol slots. The training symbols have no clipping noise and their increased energy helps reduce impairments caused by DAC noise.

A. Optical Spectrum

Fig. 5 shows the optical spectrum obtained with an Agilent high-resolution spectrometer (HRS) after 500-km of fiber. Careful adjustments of the modulator biasing, microwave path lengths, and attenuator pads were required to suppress the original laser line (in the middle of the subcarrier band) and the image of the virtual carrier that lies above the subcarrier band. The HRS's spectrum shows the 4-QAM (outer) and 16-QAM (inner) subcarrier bands, similar to Fig. 1. The spectrum also shows a small residual of the original laser line and virtual carrier image (30-dB suppression) due to small amplitude mismatches in the I and Q drive levels. Beneficially, the image of the virtual carrier falls away easily from the sideband, unlike other virtual carrier schemes.

B. Electrical SNR

Fig. 6 shows the received electrical SNR/bit for the 120 Gbit/s transmission experiment through 500-km SMF, with a 25% CP. The measured OSNR was 25.8 dB (0.1 nm) and the BER was 8.2×10^{-4}. The subcarrier's ordering is the same as the ordering in the optical spectrum in Fig. 5. In most cases, the amplitude for the optical spectrum is a useful guide for the received SNR/bit, and areas of significant difference suggested that there may be a problem with the receiver. For example, the drooping response for increasing negative frequencies is caused by an overlap in the passbands of the receiver optical filters that separate the carrier
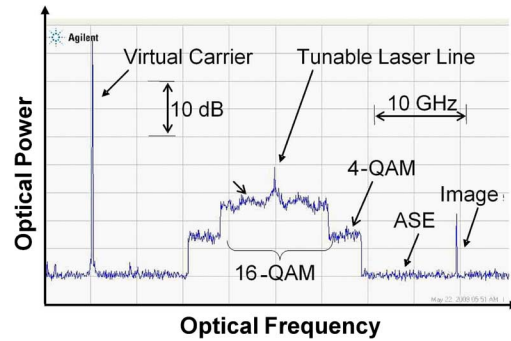
Fig. 5. Optical spectrum after 500-km of fiber, obtained with a high-resolution spectrophotometer (20-MHz resolution).
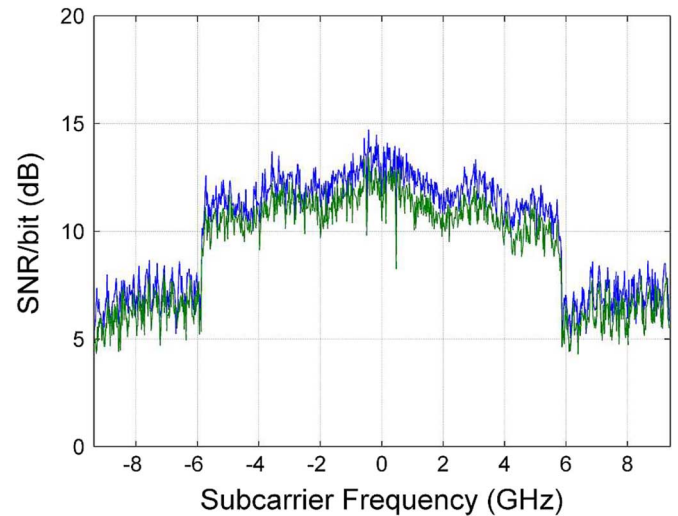
Fig. 6. Electrical SNR/bit (E_b/N_0) measured for the 120 Gbit/s transmission experiment with 500 km of SSMF, for an OSNR of 25.8 dB (0.1 nm) and 8.2×10^{-4} BER. An SNR/bit of 6.8 dB is required for a BER of 1×10^{-3} for 4 QAM and 10.6 dB is required for 16 QAM.

and the sideband. This dip can be reduced by offsetting the frequency of the carrier filter, but this leads to less carrier power and increased noise at the input to the optical hybrid. In the experiments, a compromise between filter overlap and carrier output is used to minimize the error rate.

C. Received and Equalized Constellations

Fig. 7 shows the constellations for the 4-QAM and 16-QAM subcarriers after 500-km, with the X and Y polarizations plotted in red and blue, respectively. The 4-QAM and 16-QAM constellations have similar spreads compared with their separations, indicating that they will offer similar bit error ratios.

D. BER Versus OSNR

Fig. 8 shows the BER versus OSNR plots for the optical back-to-back and 500-km transmission measurements, and simulation results from VPItransmissionMaker. The OSNR was measured with a calibrated Agilent 86142B optical spectrum analyzer set to a resolution bandwidth of 0.5 nm (to capture the whole signal power) and then rescaled to 0.1 nm (the standard bandwidth for OSNR calculations). The slightly lower power (0.7 dB) in the training sequence is accounted for, so that the
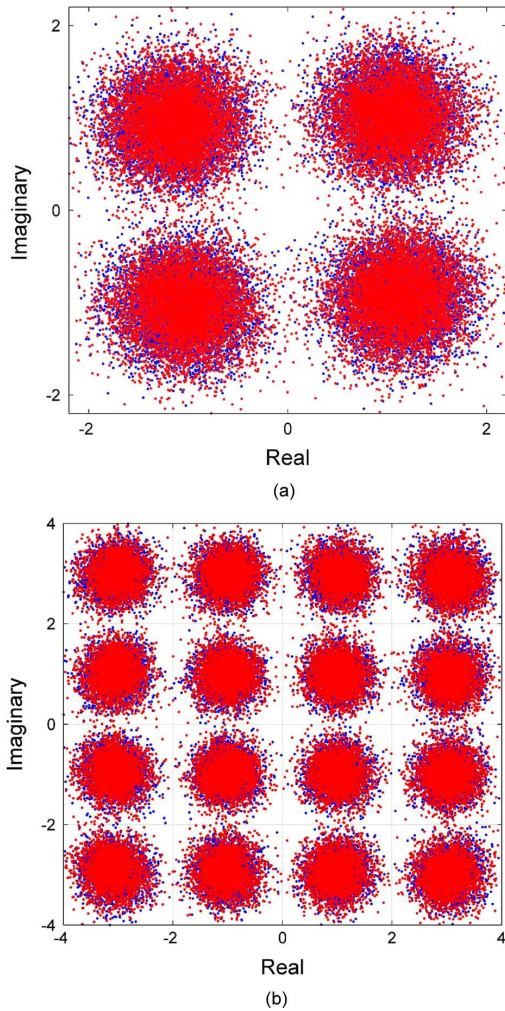
Fig. 7. Constellations for 4-QAM and 16-QAM subcarriers after 500 km of fiber. Note red points (X-polarization) are sometimes plotted over blue points (Y-polarization).
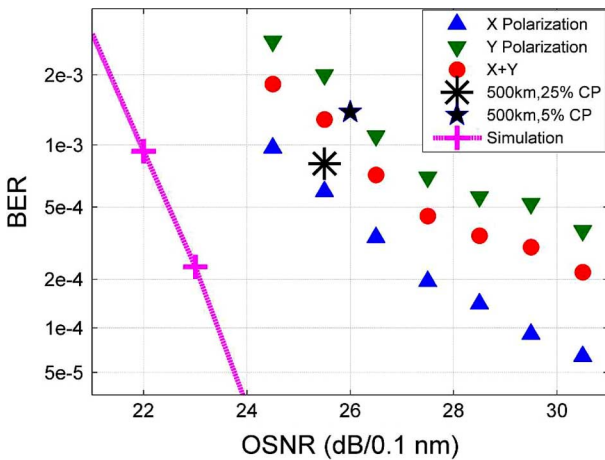
Fig. 8. BER versus OSNR plots. The line indicates simulated results, the triangles are optical back-to-back measurements, the stars indicate 500 km transmission measurements and are an average of the results of the X and Y polarizations.

OSNR accurately represents the required OSNR for a system with infrequent training.

The plots for the measured data show a tendency toward a BER floor. This is due to limitations in the AWGs' DAC performance: to increase the sample rate and the analog bandwidth, the AWGs are run in ''interleaved'' and ''zeroed'' mode. This mode provides increased bandwidth but at the expense of increased spurious noise and a halving of the output amplitude. The DAC performance is also reduced by the strong preemphasis required at high frequencies.

There is a considerable difference in the BER performance of the X and Y polarizations, shown in the optical back-to-back results in Fig. 8. This is because the data in the Y polarization have a delay of one symbol period relative to the carrier. This decorrelates the laser phase noise between the carrier and the subcarriers in the Y polarization, so the laser phase noise does not cancel effectively upon photodetection. In Fig. 8, the penalties due to the laser phase noise increase from 2 to > 4 dB as the Y polarization's BER floor is approached.

The back-to-back performance of the X polarization was within 2.5 dB of the simulated result for a BER of 1×10^{-3}. The required OSNR in the simulation, for the generally 16-QAM signal, was 21.9 dB and the experimental result was 24.3 dB. The simulation is based on the same topology as the experimental system and uses perfect components with one exception: the simulations model nonideal optical filters with bandwidths similar to the optical filters used in the experiment. The optical filter bandwidths, offset, and order have a significant effect on the OSNR requirements, and the simulation filter orders were increased to third order to ensure conservative comparisons. The experimental OSNR for 500-km transmission using a 25% CP required 25.8 dB, compared to a simulated 22.2 dB at a BER of 8.2×10^{-4}. A large part of the increased penalty from 2.5 to 3.6 dB is due to the transmission BER being an average over the BERs of the X and Y polarizations, when it might be expected that the Y channel could be improved to the X channel's performance if the additional delay is removed. The experimental OSNR for 500-km transmission using a 5% CP was 26 dB for a BER of 1.5×10^{-3}. The decreased performance was due to experimental error that led to a CP of less than 5%.

V. CONCLUSION

We have demonstrated a 120-Gbit/s self-coherent optical OFDM system capable of transmitting more than 500-km using readily available commercial components and test equipment. Only one electrical and one optical band are used at the transmitter, rather than multiplexing together individual electrical bands, optically or electrically. Several advanced design features are combined to obtain this performance. The optical transmitter uses a virtual carrier scheme to maximize the quality of the transmitted signal by placing the subcarrier bands at the center of the modulator's response. The virtual carrier can be adjusted finely to tune its frequency and amplitude by adjusting one RF signal.

At the receiver, a polarization-diverse self-coherent system was developed. This uses an optical filter to separate the carrier from the signal band, then a polarization diverse coherent heterodyne receiver with PMD compensation and polarization demultiplexing. Balanced photodiodes were used. These cancel *subcarrier* $\times$ *subcarrier* noise, which is usually a limitation to

the spectral efficiency of direct-detection systems, as a gap has to be left in the spectrum for them to fall in, upon photodetection. The new limitation is the performance of the optical filter. In the demonstration, we could reduce the gap from the signal bandwidth (19 GHz) to 8 GHz without penalty.

The OSNR requirement was close to a near-perfect system simulation. Compared with a coherent system, some additional OSNRs are required because the carrier is also transmitted along with the subcarriers. This adds 3 dB to the OSNR requirement, although carrier suppression [20] could reduce this penalty. The use of 16-QAM introduces a theoretical 3.7-dB OSNR penalty over 4-QAM. Thus, the performance is expected to be within 7-dB of coherent systems. For comparison, a recent experimental 4-QAM five-band 107 Gbit/s coherent O-OFDM system required 17 dB OSNR [11]. Improved DACs would allow our method to use 4-QAM, potentially reducing our OSNR requirement to within 4 dB of the coherent sensitivity.

REFERENCES

[1] H. Bülow, "Tutorial: Electronic dispersion compensation," presented at the Opt. Fiber Telecommun., Anaheim, CA, 2007, Paper OMG5.

[2] M. Cvijetic, "Towards 100 GbE introduction: Challenges and practical aspects," presented at the 10th Anniversary Int. Conf. Transparent Opt. Netw. 2008 (ICTON 2008), Athens, Greece, , Paper 1–4.

[3] C. R. S. Fludger, T. Duthel, D. van den Borne, C. Schulien, E. D. Schmidt, T. Wuth, J. Geyer, E. De Man, G.-D. Khoe, and H. de Waardt, "Coherent equalization and POLMUX-RZ-DQPSK for robust 100-GE transmission," *J. Lightw. Technol.*, vol. 26, no. 1, pp. 64–72, Jan. 2008.

[4] J. Yu, D. Qian, T. Wang, G. Zhang, and P. D. Magill, "8 × 114 Gb/s, 25-GHz-spaced, PolMux-RZ-8 PSK transmission over 640 km of SSMF employing digital coherent detection and EDFA-only amplification," presented at the Opt. Fiber Commun., San Diego, CA, 2008, Paper PDP1.

[5] A. J. Lowery, L. Du, and J. Armstrong, "Orthogonal frequency division multiplexing for adaptive dispersion compensation in long haul WDM systems," presented at the Opt. Fiber Commun. (OFC 2006), Anaheim, CA, , Paper PDP39.

[6] W. Shieh and C. Athaudage, "Coherent optical orthogonal frequency division multiplexing," *Electron. Lett.*, vol. 42, no. 11, pp. 587–588, May 2006.

[7] I. B. Djordjevic and B. Vasic, "Orthogonal frequency division multiplexing for high-speed optical transmission," *Opt. Exp.*, vol. 14, pp. 3767–3775, 2006.

[8] W. Shieh, "PMD-supported coherent optical OFDM systems," *IEEE Photon. Technol. Lett.*, vol. 19, no. 3, pp. 134–136, Feb. 2007.

[9] H. Takahashi, A. Al Amin, S. L. Jansen, I. Morita, and H. Tanaka, "8 × 66.8-Gbit/s coherent PDM-OFDM transmission over 640 km of SSMF at 5.6-bit/s/Hz spectral efficiency," in *Proc. 34th Eur. Conf. Opt. Commun. 2008 (ECOC)*, pp. 1–2.

[10] H. Takahashi, A. A. Amin, S. L. Jansen, I. Morita, and H. Tanaka, "DWDM transmission with 7.0-bit/s/Hz spectral efficiency using 8 × 65.1-Gbit/s coherent PDM-OFDM signals," presented at the Opt. Fiber Commun. (OFC 2009), San Diego, CA, , Paper PDPB7.

[11] W. Shieh, Q. Yang, and Y. Ma, "107 Gb/s coherent optical OFDM transmission over 1000-km SSMF fiber using orthogonal band multiplexing," *Opt. Exp.*, vol. 16, pp. 6378–6386, 2008.

[12] S. L. Jansen, I. Morita, T. C. W. Schenk, and H. Tanaka, "121.9-Gb/s PDM-OFDM transmission with 2-b/s/Hz spectral efficiency over 1000 km of SSMF," *J. Lightw. Technol.*, vol. 27, no. 3, pp. 177–188, Feb. 2009.

[13] A. D. Ellis and F. C. G. Gunning, "Spectral density enhancement using coherent WDM," *IEEE Photon. Technol. Lett.*, vol. 17, no. 2, pp. 504–506, Feb. 2005.

[14] A. Sano, E. Yamada, H. Masuda, E. Yamazaki, T. Kobayashi, E. Yoshida, Y. Miyamoto, S. Matsuoka, R. Kudo, K. Ishihara, Y. Takatori, M. Mizoguchi, K. Okada, K. Hagimoto, H. Yamazaki, S. Kamei, and H. Ishii, "13.4-Tb/s (134 × 111-Gb/s/ch) no-guard-interval coherent OFDM transmission over 3 600 km of SMF with 19-ps average PMD," in *Proc. 34th Eur. Conf. Opt. Commun. (ECOC)*, 2008, pp. 1–2, Paper 1–2.

[15] B. J. C. Schmidt, Z. Zan, L. B. Du, and A. J. Lowery, "100 Gbit/s transmission using single-band direct-detection optical OFDM," presented at the Opt. Fiber Commun. (OFC 2009), San Diego, CA, , paper PD3.

[16] B. J. C. Schmidt, A. J. Lowery, and J. Armstrong, "Experimental demonstrations of electronic dispersion compensation for long-haul transmission using direct-detection optical OFDM," *J. Lightw. Technol.*, vol. 26, no. 1, pp. 196–203, Jan. 2008.

[17] B. J. C. Schmidt, A. J. Lowery, and J. Armstrong, "Impact of PMD in single-receiver and polarization-diverse direct-detection optical OFDM," *J. Lightw. Technol.*, vol. 27, no. 14, pp. 2792–2799, Jul. 2009.

[18] D. Qian, N. Cvijetic, J. Hu, and T. Wang, "108 Gb/s OFDMA-PON with polarization multiplexing and direct-detection," presented at the Opt. Fiber Commun. (OFC 2009), San Diego, CA, , Paper PD5.

[19] B. J. C. Schmidt, A. J. Lowery, and L. B. Du, "Low sample rate transmitter for direct-detection optical OFDM," presented at the Opt. Fiber Telecommun. (OFC 2009), San Diego, CA, , Paper OWM4.

[20] A. J. Lowery, "Improving sensitivity and spectral efficiency in direct-detection optical OFDM systems," presented at the Opt. Fiber Telecommun. (OFC 2008), San Diego, CA, , Paper OMM4.

[21] A. J. Lowery and J. Armstrong, "Orthogonal frequency division multiplexing for dispersion compensation of long-haul optical systems," *Opt. Exp.*, vol. 14, pp. 2079–2084, 2006.

[22] S. L. Jansen, I. Morita, N. Tadeka, and H. Tanaka, "20-Gb/s OFDM transmission over 4 160-km SSMF enabled by RF-pilot tone phase noise compensation," presented at the Opt. Fiber Telecommun., Anaheim, CA, 2007, Paper PDP15.

[23] X. Yi, W. Shieh, and Y. Ma, "Phase noise effects on high spectral efficiency coherent optical OFDM transmission," *J. Lightw. Technol.*, vol. 26, no. 10, pp. 1309–1316, May 2008.

[24] B. J. C. Schmidt, A. J. Lowery, and J. Armstrong, "Experimental demonstrations of 20 Gbit/s direct-detection optical OFDM and 12 Gbit/s with a colorless transmitter," presented at the Opt. Fiber Commun., Anaheim, CA, 2007, Paper PDP18.

[25] W.-R. Peng, X. Wu, V. R. Arbab, B. Shamee, L. C. Christen, J.-Y. Yang, K.-M. Feng, A. E. Willner, and C. Sien, "Experimental demonstration of a coherently modulated and directly detected optical OFDM system using an RF-tone insertion," presented at the Opt. Fiber Commun., San Diego, CA, 2008, Paper OMU2.

[26] A. J. Lowery, "Amplified-spontaneous noise limit of optical OFDM lightwave systems," *Opt. Exp.*, vol. 16, pp. 860–865, 2008.

[27] L. Xu, J. Hu, D. Qian, and T. Wang, "Coherent optical OFDM systems using self optical carrier extraction," presented at the Opt. Fiber Commun. (OFC 2008), San Diego, CA, , .

[28] C. Xie, "PMD insensitive direct-detection optical OFDM systems using self-polarization diversity," presented at the Opt. Fiber Commun. (OFC 2008), San Diego, CA, , .

[29] A. Carena, V. Curri, P. Poggiolini, and F. Forghieri, "Dynamic range of single-ended detection receivers for 100 GE coherent PM-QPSK," *IEEE Photon. Technol. Lett.*, vol. 20, no. 15, pp. 1281–1283, Aug. 2008.

[30] S. T. Chung and A. J. Goldsmith, "Degrees of freedom in adaptive modulation: A unified view," *IEEE Trans. Commun.*, vol. 49, no. 9, pp. 1561–1571, Sep. 2001.

[31] X. Liu and F. Buchali, "Intra-symbol frequency-domain averaging based channel estimation for coherent optical OFDM," *Opt. Exp.*, vol. 16, pp. 21944–21957, 2008.

Brendon J. C. Schmidt received the B.Eng. degree (first class hons) in electrical and computer systems engineering from Monash University, Melbourne, Australia in 2006, where he is currently working towards the Ph.D. degree.

His research interests include OFDM in optical communications applications.
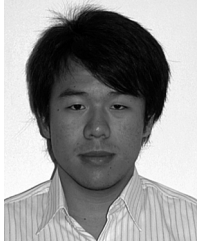
Liang Bangyuan Du was born in Shengyang, China, in 1985. He received the B.Eng. degree (Hons) and commerce majoring in electrical and computer engineering and finance, respectively, from Monash University, Melbourne, Australia, where he is currently working towards the Ph.D. degree in the Department of Electrical and Computer Systems Engineering.

His research interests include optical orthogonal frequency division multiplexing and fiber nonlinearity.

Zuraidah Zan received the B.Eng. degree (Hons) in computer and communication systems from Universiti Putra Malaysia, Malaysia, in 2003, and the M.Sc. degree in communication engineering from Universiti Kebangsaan Malaysia, Malaysia, in 2006y. She is currently working toward the Ph.D. degree at Monash University, Melbourne, Australia with her major area of research being the optical orthogonal frequency division multiplexing system.

Arthur James Lowery (M'91–SM'96–F'09) was born in Yorkshire, England, in 1961. He received the B.Sc. degree (first class hons) in applied physics from the University of Durham, U.K., in 1983 and the Ph.D. degree in electrical and electronic engineering from the University of Nottingham, Nottingham, U.K., in 1988.

In 1984 he joined the University of Nottingham as a lecturer and pioneered time-domain field modelling of semiconductor lasers as the Transmission-Line Laser Model. In 1990 he emigrated to Australia to become a Senior Lecturer at the Photonics Research Laboratory at the University of Melbourne. After working on Photonic-CAD, Packet Switching and Laser Ranging, he was promoted to Associate Professor and Reader in 1993. He continued to develop novel time-domain simulation techniques and in 1996 he co-founded Virtual Photonics Pty Ltd. Virtual Photonics merged with BNeD (Berlin) in 1998, with Lowery as CTO, leading the development of VPI's physical-level photonic design automation tools such as VPItransmissionMaker and VPIcomponentMaker, which are widely used in industry and academia for development, research and teaching. In 2004 he was appointed Professor of Electrical and Computer Systems Engineering at Monash University, Melbourne, Australia where he is working on the applications of photonic technology, including a bionic vision device. In 2008 he founded Ofidium Pty Ltd to commercialise optical OFDM. He has published more than 200 papers and 4 book chapters on the simulation of photonic devices and circuits and photonic applications such as mode-locking, packet switching, OFDM transmission systems and high-speed photonic circuits.

Prof. Lowery is a Fellow of the IEEE, the IET (UK) and the Australian Academy of Technological Sciences and Engineering (ATSE), from which he received a 2007 Clunies-Ross Award for his work on photonic simulation.